

Steady-state velocity distributions of an oscillated granular gas

Sung Joon Moon,* J. B. Swift,† and Harry L. Swinney‡

Center for Nonlinear Dynamics and Department of Physics, University of Texas, Austin, Texas 78712, USA

(Received 25 March 2003; published 14 January 2004)

We use a three-dimensional molecular dynamics simulation to study the single particle distribution function of a dilute granular gas driven by a vertically oscillating plate at high accelerations (15g–90g). We find that the density and the temperature fields are essentially time-invariant above a height of about 40 particle diameters, where typically 20% of the grains are contained. These grains form the nonequilibrium steady-state granular gas with a Knudsen number unity or greater. In the steady-state region, the probability distribution function of the horizontal velocity c_x (scaled by the local horizontal temperature) is found to be nearly independent of height, even though the hydrodynamic fields vary with height. We find that the high energy tails of the distribution function are described by a stretched exponential $\sim \exp(-\mathcal{B}c_x^\alpha)$, where α depends on the restitution coefficient e and falls in the range $1.2 < \alpha < 1.6$. However, α does not vary significantly for a wide range of friction coefficient values. We find that the distribution function of a *frictionless* inelastic hard sphere model can be made similar to that of a frictional model by adjusting e . However, there is no single value of e that mimics the frictional model over a range of heights.

DOI: 10.1103/PhysRevE.69.011301

PACS number(s): 45.70.-n, 05.20.Dd, 05.70.Ln, 83.10.Rs

I. INTRODUCTION

A dilute gas in thermal equilibrium is sufficiently characterized by the pressure and temperature and is described by a simple relation, the equation of state. However, when a gas is far from equilibrium, there is no general, finite set of variables specifying the state. The single particle distribution function $f(\mathbf{r}, \mathbf{v}, t)$ is often sufficient to characterize the statistical properties of a dilute nonequilibrium gas when correlations are negligible. Given this function, other quantities, such as moments of the distribution and transport coefficients, can be evaluated. Dilute granular materials subject to an external forcing exhibit gaseous behaviors that share many analogies with a molecular gas, and they are often called granular gases. Such a granular gas is always far from equilibrium due to the dissipative collisions, and the deviation of $f(\mathbf{r}, \mathbf{v}, t)$ from the Maxwell-Boltzmann (MB) distribution has been of great interest in recent years [1–5].

Warr *et al.* [1] studied the velocity distribution functions of vibrofluidized grains confined between two transparent plates and concluded that the distribution was consistent with the MB distribution function. Recently, the same system subject to stronger forcing has been studied by Rouyer and Meunier [5]. They found a *universal* distribution function of the horizontal velocity v_x (of grains in a rectangular or circular region around the center of the container, where density did not vary much in height or time) of the form $\sim \exp(-B|v_x|^{1.55})$ for the *entire* range of velocities, where B was determined by the granular temperature of all the sampled grains. The authors reported that this functional form described their measurements for a wide range of density, temperature, and all the oscillation parameters investigated; thus

the granular temperature was the only parameter of the distribution function.

There have been numerical studies of vibrated inelastic hard disks, subject to a sawtooth type oscillation, in the presence of gravity [6] and in the absence of gravity [7]. Such forcing is often used in theoretical studies as a simplification of the sinusoidal oscillation used in experiments, assuming that the asymptotic behavior of the hydrodynamic fields far from the plate is the same. However, it is not known *a priori* how far from the oscillating plate one must be in order for this assumption to be valid.

In this paper, we use a previously validated molecular dynamics (MD) simulation [8,9]. The hydrodynamic fields are oscillatory near the plate, and their oscillatory behavior decays with height. Above some height, the fields are not correlated with the oscillation of the plate and are essentially time invariant. We study the distribution functions in this nonequilibrium steady-state region. To focus on the distributions due to the intrinsic dynamics of the granular gas, we do not impose sidewalls or include air. We also study how the distribution changes with the friction. In many theoretical or numerical studies of granular fluids, granular materials are modeled as frictionless inelastic hard disks or spheres; however, no granular materials are frictionless, in the same way that none of them are elastic. We check if the role of friction can be incorporated into the inelasticity by adjusting the value of the normal coefficient of restitution.

In this paper we discuss the distributions only in the steady-state region; those in the oscillatory region near the plate will be discussed in a separate paper [10]. The rest of the paper is organized as follows. In Sec. II, the system under consideration, the data analysis method, and the collision model are described. Results are presented in Sec. III and discussed in Sec. IV.

II. METHOD

A. System and data analysis

We use both a frictional and frictionless inelastic hard sphere MD simulation. We consider 133 328 monodisperse

*Electronic address: moon@chaos.utexas.edu

†Electronic address: swift@chaos.utexas.edu

‡Electronic address: swinney@chaos.utexas.edu

spheres of unit mass and of diameter $\sigma = 165 \mu\text{m}$ in a container with square bottom of area $200\sigma \times 200\sigma$ (the average depth of the layer at rest is approximately 3σ), where periodic boundary conditions are imposed in both horizontal directions. We choose the same particle size as in Ref. [8], as the patterns were quantitatively reproduced for a wide range of oscillation parameters with this particle size; however, as long as the collision model is valid, all the length scales can be normalized by σ . We assume the bottom plate of the container is made of the same material as grains. We use the same coefficients of restitution and friction for grain-bottom collisions as for grain-grain collisions. The bottom plate is subject to a vertical sinusoidal oscillation with an amplitude A and a frequency f . We vary the oscillation parameters in the range of $3\sigma < A < 10\sigma$ and $40 \text{ Hz} < f < 170 \text{ Hz}$, which approximately corresponds to $0.35 \text{ m/s} < V_{max} (= 2\pi f A) < 0.75 \text{ m/s}$ and $15g < a_{max} [= A(2\pi f)^2] < 90g$, where g is the acceleration due to gravity. We check that with our parameters no mean flow develops and that grains rarely reach to the top, which is fixed at 300σ .

Hydrodynamic fields and the distribution functions are analyzed by binning the box into horizontal slabs of height σ , as the system is invariant under translation in both horizontal directions, in the absence of any mean flow. We use the granular volume fraction ν for the density, which is the ratio of the volume occupied by grains to the volume of each horizontal slab. We consider the following three granular temperatures separately in each slab:

$$T_x = \frac{1}{2} \langle (v_x - \langle v_x \rangle)^2 + (v_y - \langle v_y \rangle)^2 \rangle, \quad (1)$$

$$T_z = \langle (v_z - \langle v_z \rangle)^2 \rangle, \quad (2)$$

$$T = \frac{1}{3} \langle |\mathbf{v} - \langle \mathbf{v} \rangle|^2 \rangle \quad (3)$$

$$= \frac{1}{3} (2T_x + T_z), \quad (4)$$

where x and y are horizontal directions that are indistinguishable, z is the vertical direction, \mathbf{v} is a velocity vector for each grain, and the ensemble average $\langle \rangle$ is taken over the particles in the same bin at the same phase angle during 40 cycles, after initial transients have decayed. We define the scaled horizontal velocity to be

$$c_x = (v_x - \langle v_x \rangle) / \sqrt{2T_x}. \quad (5)$$

B. Collision model

We implement the collision model that was originally proposed by Maw *et al.* [11], simplified by Walton [12], and then experimentally tested by Foerster *et al.* [13]. This model updates the velocity after a collision according to the three parameters—the normal coefficient of restitution e ($\in [0,1]$), the coefficient of friction μ which relates the tangential force to the normal force at collision using Coulomb's law and then determines the tangential coefficient of restitution β ($\in [-1,1]$), and the maximum tangential coefficient of restitution β_0 which represents the tangential restitution of the surface velocity when the colliding particles slide discontinuously at the contact point.

At collision, it is convenient to decompose the relative colliding velocities into the components normal (\mathbf{v}_n) and tangential (\mathbf{v}_t) to the normalized relative displacement vector $\hat{\mathbf{r}}_{12} \equiv (\mathbf{r}_1 - \mathbf{r}_2) / |\mathbf{r}_1 - \mathbf{r}_2|$, where \mathbf{r}_1 and \mathbf{r}_2 are displacement vectors of grains 1 and 2, and the same rule for the notation is used for \mathbf{v}

$$\mathbf{v}_n = (\mathbf{v}_{12} \cdot \hat{\mathbf{r}}_{12}) \hat{\mathbf{r}}_{12} \equiv v_n \hat{\mathbf{r}}_{12}, \quad (6)$$

$$\mathbf{v}_t = \hat{\mathbf{r}}_{12} \times (\mathbf{v}_{12} \times \hat{\mathbf{r}}_{12}) = \mathbf{v}_{12} - \mathbf{v}_n. \quad (7)$$

The relative surface velocity at collision \mathbf{v}_s for monodisperse spheres of diameter σ is

$$\mathbf{v}_s = \mathbf{v}_t + \frac{\sigma}{2} \hat{\mathbf{r}}_{12} \times (\mathbf{w}_1 + \mathbf{w}_2) \equiv v_s \hat{\mathbf{v}}_s, \quad (8)$$

where \mathbf{w}_1 and \mathbf{w}_2 are the angular velocities of grains 1 and 2, respectively.

For monodisperse spheres of diameter σ and unit mass, the linear and angular momenta conservation and the definitions of the normal coefficient of restitution $e \equiv -v_n^*/v_n$ and the tangential coefficient of restitution $\beta \equiv -v_s^*/v_s$ (postcollisional velocities are indicated by superscript *, and precollisional values have no superscript) give the changes in the velocities at the collision:

$$\Delta \mathbf{v}_{1n} = -\Delta \mathbf{v}_{2n} = \frac{1}{2} (1 + e) \mathbf{v}_n, \quad (9)$$

$$\Delta \mathbf{v}_{1t} = -\Delta \mathbf{v}_{2t} = \frac{K(1 + \beta)}{2(K + 1)} \mathbf{v}_s, \quad (10)$$

$$\Delta \mathbf{w}_1 = -\Delta \mathbf{w}_2 = \frac{(1 + \beta)}{\sigma(K + 1)} \hat{\mathbf{r}}_{12} \times \mathbf{v}_s, \quad (11)$$

where $K = 4I/\sigma^2$ is a geometrical factor relating the momentum transfer from the translational degrees of freedom to rotational degrees of freedom, and I is the moment of inertia about the center of the grain. For a uniform density sphere, K is $2/5$.

We use a velocity-dependent normal coefficient of restitution as in Ref. [8], to account for the viscoelasticity of the real grains:

$$e = \max \left[e_0, 1 - (1 - e_0) \left(\frac{v_n}{\sqrt{g\sigma}} \right)^{3/4} \right], \quad (12)$$

where e_0 is a positive constant less than unity. Since we impose high forcing ($V_{max} > 0.35 \text{ m/s}$ while $\sqrt{g\sigma} = 0.04 \text{ m/s}$) the collision probability for relative colliding velocities v_n less than $\sqrt{g\sigma}$ is small, and using a velocity dependent e does not result in any noticeable difference, compared to using a velocity independent one $e = e_0$; the same was true in Ref. [14]. We use the symbol e for e_0 hereafter.

In collisions of real granular materials, not only is the relative surface velocity reduced, but also the stored tangential strain energy in the contact region can often reverse the

direction of the relative surface velocity. To account for this effect, the tangential coefficient of restitution β could be positive, leading to the range of β as $[-1, 1]$. There are two kinds of frictional interaction at collisions, sliding and rolling friction, which are accounted for by the following formula for β :

$$\beta = \min \left[\beta_0, -1 + \mu(1+e) \left(1 + \frac{1}{K} \frac{v_n}{v_s} \right) \right], \quad (13)$$

where β_0 is the maximum tangential coefficient of restitution. For sliding friction, the tangential impulse is assumed to be the normal impulse multiplied by μ . When β is identically negative unity (or simply $\mu=0$), this model reduces to the frictionless interaction. For the special case $v_s=0$, the collision is treated as frictionless. This friction model is still a simplification of the frictional interaction in experiments; there is no clear-cut distinction between the two types of frictions for real grains, and even a transfer of energy from the rotational to translational degrees of freedom, which results in e larger than unity, has been observed [15]. However, this collision model is accurate enough to reproduce many phenomena, including standing wave pattern formation in vertically oscillated granular layers, when the parameters are properly chosen. In Refs. [8] and [9], $e=0.7$, $\beta_0=0.35$, and $\mu=0.5$ were used.

III. RESULTS

A. Hydrodynamic fields and steady state

Due to the oscillatory boundary forcing the hydrodynamic fields, the volume fraction ν and the granular temperatures (T , T_x , and T_z) depend on height z and time t (Fig. 1) near the oscillating plate; the temperatures exhibit stronger oscillatory behavior than the density. Since the energy is injected mainly through the vertical velocities, the granular temperature is anisotropic as illustrated in Fig. 1; T_z is larger than its horizontal counterpart T_x , and the former is significantly larger near the bottom plate, where the hydrodynamic fields are oscillatory. The vertical temperature increases almost linearly with height for $z/\sigma > 40$; however, the temperature T increases more slowly than linearly, as the slope of T_x decreases with height and T_x levels off for $z/\sigma > 120$ (Fig. 1). A similar increase of the temperature with height was observed in an open system of frictionless inelastic hard disks or spheres subject to a thermal bottom heating [16] and a sawtooth-type vibration [17]. We characterize the oscillation parameters only by V_{max} , as we observe for the parameters in our study that the hydrodynamic fields in the steady state are nearly the same for the same V_{max} , even for different combinations of a_{max} and f ; such scaling behavior was also observed in Ref. [18].

During each cycle, a normal shock forms at the impact from the bottom plate and propagates upward [14]. As the shock propagates, it decays and becomes undetectable above some height ($z/\sigma \approx 40$), rather than propagating up through the entire granular media (which was the case in Ref. [14]). Above this height, the hydrodynamic fields are invariant in time, and the granular gas forms a nonequilibrium steady

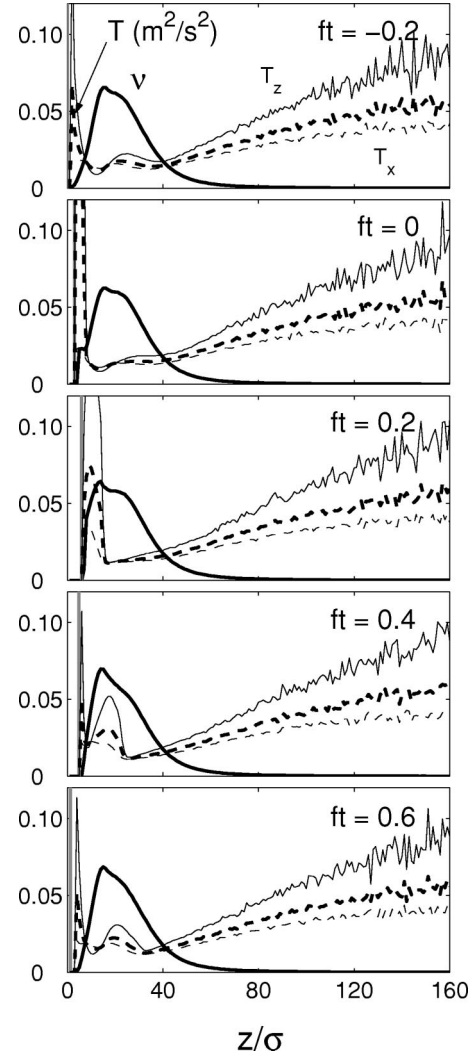


FIG. 1. The volume fraction ν (thick solid line) and the granular temperature T (thick dashed line) as a function of height at different times during a cycle, where $e=0.9$, $\beta_0=0.35$, $\mu=0.5$, $V_{max}=0.55$ m/s ($a_{max}=60g$, $A=3\sigma$, and $f=169$ Hz), and ft is set to zero when the plate is at the equilibrium position ($z=A$) moving upward; the plate oscillates between 0 and $2A$. Above some height ($z/\sigma \approx 40$), the hydrodynamic fields do not vary much in time. The horizontal temperature T_x (thin dashed line) is smaller than the vertical temperature T_z (thin solid line). The vertical gray line indicates the container bottom.

state (Fig. 2). About 20% of the grains are contained in this region for the oscillation parameters of Fig. 1.

With the parameters used in this paper the granular temperatures are nonzero throughout the cycle, as grains do not solidify after the shock passes through, in contrast to the case in Ref. [14]. As a result, when the bottom plate moves down, the granular gas expands, and an expansion wave propagates downward (see the temperature peaks near the plate for $ft > 0.4$ in Fig. 1).

We count the number of grain-grain collisions per grain during a cycle (N_{coll} in Fig. 3), and find that N_{coll} is less than unity in the steady-state region; the granular gas in the steady state is nearly collisionless. We estimate the mean free

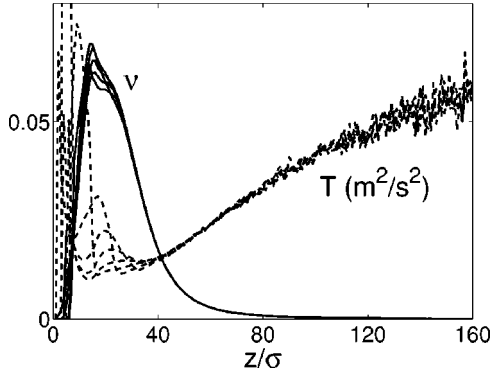


FIG. 2. This superposition of the volume fraction and temperature fields at five different times in a cycle (see Fig. 1) illustrates that the fields are nearly time independent above $z/\sigma \approx 40$, which we call the steady-state region.

path using the formula for a gas of hard spheres $\lambda(z)/\sigma = (2\sqrt{2}\pi n\sigma^3)^{-1} = \sqrt{\pi}/(12\sqrt{2}\nu)$ (where n is the number density) [19], which ranges between 5 and 280 for $40 < z/\sigma < 100$ (Fig. 4). When we estimate the mean free path using the measured collision frequency and the thermal speed, we get a similar result. We fit the density with piecewise exponential functions [$\sim \exp(-(z-z_0)/l_\nu)$] in the steady state region, and obtain a hydrodynamic length scale l_ν/σ between 12 and 15 for $40 < z/\sigma < 100$. We obtain a similar length scale from piecewise linear fitting of the temperature T in the same region. We calculate the Knudsen number Kn , defined as the ratio of the mean free path to the length scale of the macroscopic gradients [20], using $\lambda(z)$ and l_ν ; Kn ranges from 0.5 to 20 in the region $40 < z/\sigma < 100$ (Fig. 4).

B. Height independence of the distribution

The distribution of scaled horizontal velocities should be symmetric as a consequence of the symmetry of the system.

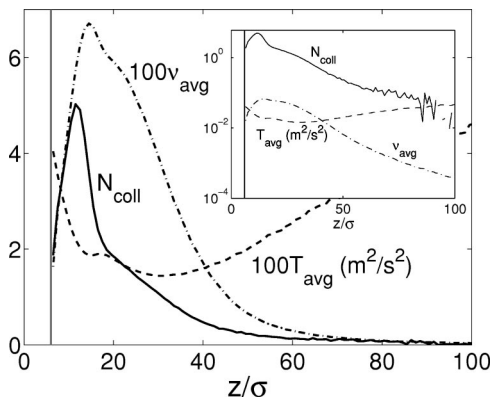


FIG. 3. The number of grain-grain collisions per grain during a cycle N_{coll} (solid line), time-averaged (over sixty different equally spaced times during a cycle) volume fraction ν_{avg} (dot-dashed line, multiplied by 100), and time-averaged granular temperature T_{avg} (dashed line, multiplied by 100). They are plotted only for $z > 2A$ (vertical gray line), where grains are present throughout the cycle. Inset: The same quantities (without multiplications) on a logarithmic scale.

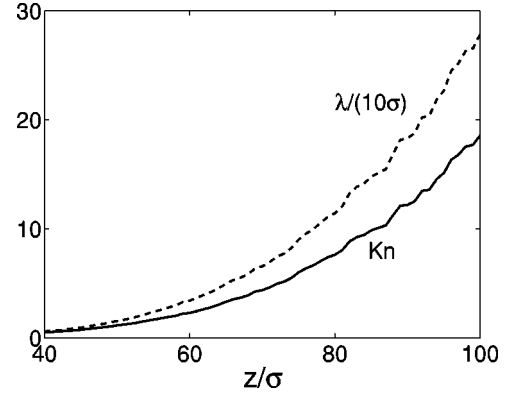


FIG. 4. The mean free path λ , estimated from a formula for a gas of hard spheres, and the Knudsen number Kn , estimated by using λ and the length scale of the density l_ν (see text), in the steady-state region.

We calculate the skewness of the distribution, $\gamma_3 = \mathcal{M}_3/\mathcal{M}_2^{3/2}$, where \mathcal{M}_n is the n th moment of the distribution

$$\mathcal{M}_n = \int c_x^n f(c_x) dc_x, \quad (14)$$

and check that $|\gamma_3|$ is less than 0.01 for all the distributions we study. The lowest order deviation from the MB distribution is characterized by the flatness of the distribution, which is called the fourth cumulant or the kurtosis. It was used to quantify the deviation from the MB distribution of the homogeneously cooling state [21–23], the homogeneously heated state [21,24], and granular gases subject to a boundary forcing [6,25]. The kurtosis $\gamma_4 (\equiv \mathcal{M}_4/\mathcal{M}_2^2 - 3)$ is defined so that it vanishes for the MB distribution, and we find that it also does not change in time above some height (Fig. 5). Further, in the steady state region γ_4 is nearly independent of the height, even though both the density and the temperature change; the distributions at different heights in the steady-state region are hardly distinguishable (Fig. 6). Also, the kurtosis in the steady-state region does not vary

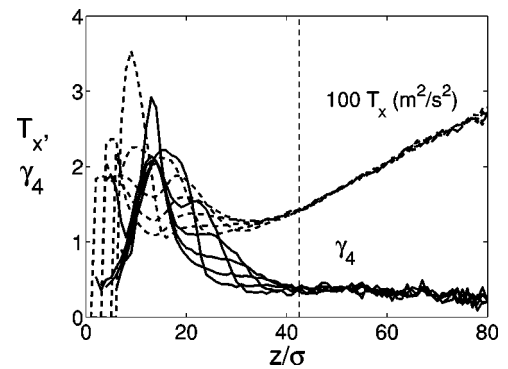


FIG. 5. Above some height ($z/\sigma \approx 40$, indicated by a vertical dashed line), the kurtosis γ_4 is nearly time-invariant. The horizontal granular temperature T_x (dashed lines) and γ_4 (solid lines) of the horizontal velocity distribution function are shown at five different equally spaced times during a cycle (cf. Fig. 1).

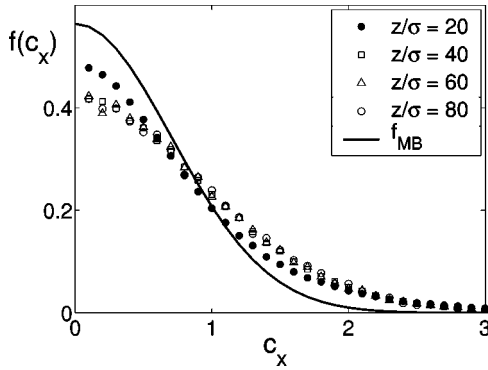


FIG. 6. The horizontal velocity distribution functions at four different heights (compared with f_{MB} , the solid line) obtained at $ft = -0.2$. There is no noticeable difference among the distributions in the steady-state region, $40 < z/\sigma < 80$.

much for a wide range of the oscillation parameters: for $0.35 \text{ m/s} < V_{max} < 0.75 \text{ m/s}$ (while other parameters are fixed), γ_4 changes less than 10%. A similar absence of height dependence of the velocity distribution function was found in a recent experiment on a vertically oscillated quasi-two-dimensional granular gas [26].

C. Velocity distributions

We first examine the dependence of the distribution on e ; we compute γ_4 for three different values of e , while β_0 and μ are kept at 0.35 and 0.5, respectively. We find that γ_4 significantly decreases with increasing e in the oscillatory state; however, it decreases only slightly in the steady state region (Fig. 7).

Now we compare our results with the MB distribution of variance $1/\sqrt{2}$,

$$f_{MB}(c_x) = \frac{1}{\sqrt{\pi}} \exp(-c_x^2). \quad (15)$$

The steady-state distributions obtained for the parameters in Fig. 7 are overpopulated in the high energy tails and under-

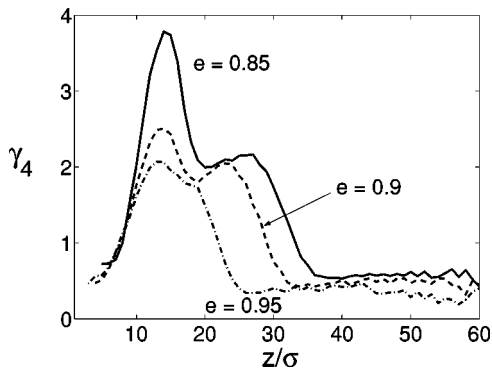


FIG. 7. Kurtosis for three values of e , as a function of height at $ft = -0.2$, where μ and β_0 are set to 0.5 and 0.35. Different forcings are applied for each case to achieve similar profiles of the hydrodynamic fields: $V_{max}(a_{max}) = 0.4 \text{ m/s}$ (43g), 0.55 m/s (60g), and 0.66 m/s (72g) for $e = 0.95$, $e = 0.9$, and $e = 0.85$, respectively.

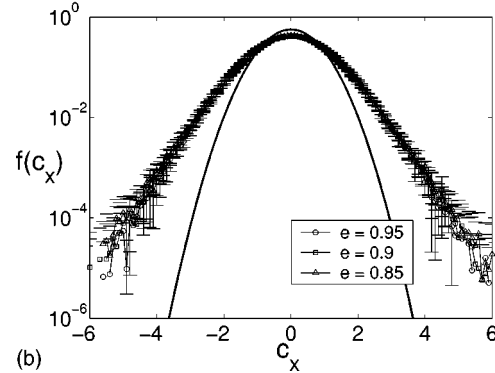
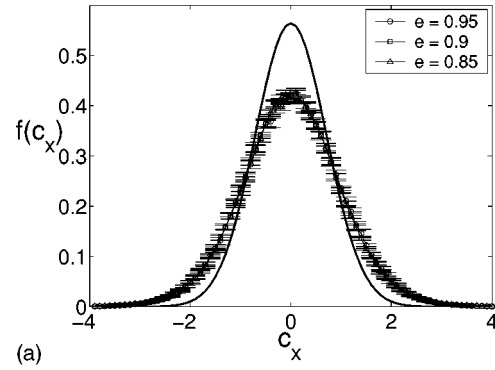


FIG. 8. The distribution functions of scaled horizontal velocities $f(c_x)$ for the cases in Fig. 7, on linear (top panel) and logarithmic (bottom panel) scales. Although the kurtosis slightly decreases with e , the difference between the distributions is hardly distinguishable on either scale. The ranges for the averaging in height were between 30σ and 45σ for $e = 0.95$, 40σ and 55σ for $e = 0.9$, and 45σ and 60σ for $e = 0.85$ (see Fig. 7). The solid line is the MB distribution.

populated at small velocities (Fig. 8), compared to f_{MB} . The differences of the distributions for various e 's are hardly noticeable either on linear or logarithmic scale (Fig. 8), but on a double logarithmic scale plot the tails of the distributions are described by different functions (Fig. 9). We investigate the functional form of the distributions by fitting them (after the normalization by the value at $c_x = 0$) with a stretched exponential function $\exp(-c_x^\alpha)$. We find that the exponent α changes from 1.9 (indicated by dashed lines) to some smaller value (solid lines), depending on e , as the velocity increases. We have not investigated lower values of e to avoid issues such as cluster formation.

We now keep e and β_0 at 0.9 and 0.35, respectively, and change the value of μ . The profile of γ_4 in the oscillatory region changes significantly with μ ; however, it is nearly unchanged in the steady state region (Fig. 10). The velocity distributions in this region for three different values of μ in Fig. 10 are also hardly distinguishable. We observe that the distribution function depends also on the density, as in Refs. [6,7,24]; however, we do not investigate this dependency systematically.

D. Frictionless inelastic hard sphere model

In theoretical and numerical studies, granular materials are often modeled as smooth (frictionless) inelastic hard

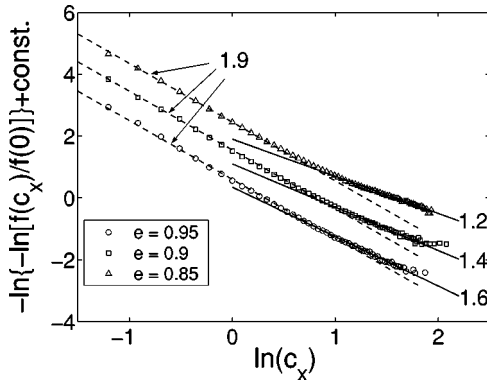


FIG. 9. Double logarithm of the distributions of scaled horizontal velocities for the cases in Fig. 7 as a function of the logarithm of c_x . The slope corresponds to the negative exponent $-\alpha$ of a stretched exponential function $\exp(-c_x^\alpha)$. α is the same for small velocities for three cases of different e 's; however, it depends on e in high energy tails. Dashed lines correspond to $\alpha=1.9$, and the solid lines (from the top) correspond to $\alpha=1.2$, 1.4, and 1.6, respectively (indicated by the numbers).

disks or spheres, assuming that the friction is a secondary effect that can be neglected or that both the inelasticity and the friction can be incorporated together into the so-called effective coefficient of restitution. In this section, we discuss how the velocity distribution changes when the friction is not included, and we show that the frictionless model exhibits qualitative differences from the frictional model.

The rotational kinetic energy is two orders of magnitude smaller than its translational counterpart for the cases studied in this paper. However, the presence of the friction reduces the expansion of the granular gas significantly, because the friction reduces the mobility of the grains and increases the collision frequency [27]. The mean height of frictional inelastic hard spheres exhibits a different scaling behavior with the plate velocity from that of frictionless spheres. Only the frictional sphere model reproduces the experimental observations [27,28].

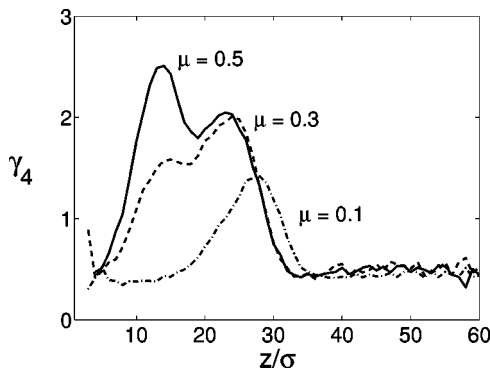


FIG. 10. Kurtosis of the scaled horizontal velocity distributions as a function of height at $ft = -0.2$ for three values of μ (β_0 and e are kept at 0.35 and 0.9, respectively). In the oscillatory region, γ_4 increases with μ ; however, γ_4 is nearly the same within the uncertainty in the steady-state region. The same forcing ($V_{max}=0.55$ m/s) is applied to the three cases.

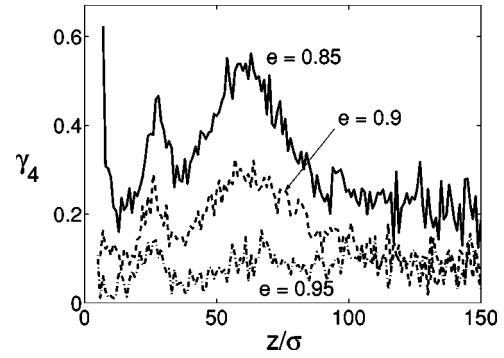


FIG. 11. Kurtosis of the distributions of scaled horizontal velocities of frictionless spheres, as a function of height for three values of e obtained at $ft = -0.2$. Different forcings (the same as in Fig. 7) are applied for each case: V_{max} (a_{max}) = 0.4 m/s (43g), 0.55 m/s (60g), and 0.66 m/s (72g) for $e=0.95$, $e=0.9$, and $e=0.85$, respectively.

The γ_4 's obtained from the simulations of frictionless particles for the same forcings as in Fig. 7 are illustrated in Fig. 11. In the absence of friction the layer expands much more, and the steady state occurs at greater height, $z/\sigma > 100$. In both the oscillatory and the steady state regions, values of γ_4 are smaller than those of frictional spheres (compare Fig. 11 with Figs. 7 and 10); the distribution deviates from f_{MB} only slightly. The kurtosis decreases with increasing e , and the difference among the distributions for the three e 's are small. These distributions have four crossovers with f_{MB} ; they are overpopulated both at very small and high velocities and are underpopulated in between, compared to f_{MB} . We fit them with a stretched exponential function, and find that α is 2.0 for small velocities, and that it depends on e for the high energy tails (Fig. 12), as in frictional inelastic hard spheres.

Since the functional form of the distribution depends on e , we can obtain a similar distribution function for the steady state by adjusting e . For instance, for $\mu=0$, $e=0.7$, and $V_{max}=0.55$ m/s (the same forcing as in Fig. 7) we obtain $\gamma_4 \approx 0.5$ for the steady-state region; the steady-state distribution is similar to the one in Fig. 7 for $e=0.9$ and $\mu=0.5$.

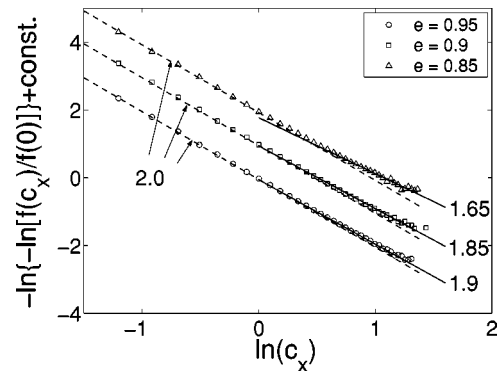


FIG. 12. Double logarithm of the rescaled horizontal velocity distribution functions (normalized by its value at zero) for the cases in Fig. 11, as a function of the logarithm of c_x . Dashed lines correspond to $\alpha=2.0$, and the solid lines (from the top) correspond to $\alpha=1.65$, 1.85, and 1.9, respectively.

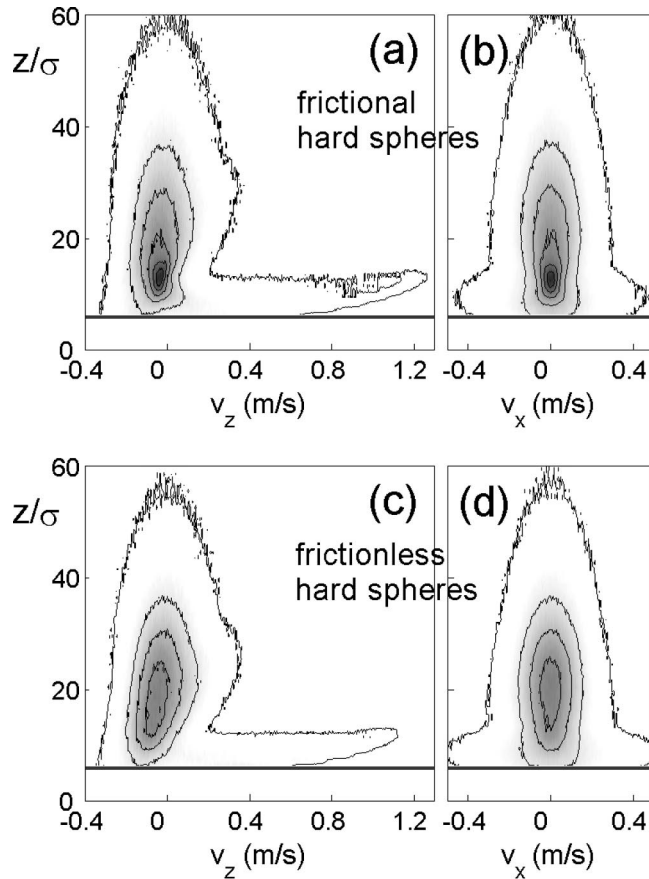


FIG. 13. The volume fraction ν (gray scale and contour lines) at $ft=0.25$ as a function of height and v_z [(a) and (c)], and of height and v_x [(b) and (d)], obtained from simulations of frictional hard spheres [(a) and (b); $e=0.9, \mu=0.5$], and of frictionless hard spheres [(c) and (d); $e=0.7, \mu=0$] at $V_{max}=0.55$ m/s; e is adjusted in the frictionless case to obtain comparable overall dissipation and similar velocity distribution functions in the steady-state region. The frictionless spheres spread more smoothly in height, and they do not yield the sharp gradient in the density around $z/\sigma \approx 13$ as in the frictional case, no matter what the value of e is; the density profile of the frictionless spheres is qualitatively different from that of frictional spheres. Contour lines correspond to $(0.03, 0.3, 0.6, 0.9, 1.2, 1.5) \times 10^{-3}$ from outside.

However, we find that no single value of e mimics the hydrodynamic fields or the distribution function of frictional inelastic hard spheres, both in the oscillatory and steady state regions; the effect of friction cannot be taken over by an adjusted normal coefficient of restitution. The difference between the results of the two models is illustrated in Fig. 13, where velocities are not rescaled for better comparison. The outermost contour lines in both models become similar when e in the frictionless model is adjusted as a free parameter [compare Figs. 13(a) and 13(c), or 13(b) and 13(d)]; however, the overall shape of the density contours cannot be matched by adjusting only e . Note that the density changes rapidly with height and $\nu > 1.5 \times 10^{-3}$ at $z/\sigma \approx 10$ near $v_z \approx v_x \approx 0$ in the frictional model, whereas in the frictionless model the particles spread more smoothly in height and there is no region of $\nu > 1.2 \times 10^{-3}$.

IV. CONCLUSIONS

We have studied the horizontal velocity distribution function of vertically oscillated dilute granular gas using a molecular dynamics simulation of frictional inelastic hard spheres. The hydrodynamic fields are oscillatory in time near the oscillating bottom plate due to a shock wave and an expansion wave. However, the fields are nearly stationary above some height, thus constituting a granular gas in a non-equilibrium steady-state. The steady state region forms a granular analog of a nearly collisionless Knudsen gas (Figs. 3 and 4). We find that the dependence of the distribution functions in this granular Knudsen gas regime on the forcing and material parameters is very weak, even though the distributions in the collisional bulk at lower heights depend strongly on the forcing and material parameters (Figs. 7 and 10). The behavior of an ordinary Knudsen gas is determined by boundary conditions [20]. Although we do not know whether boundary conditions or collisions are dominant in determining the behavior of our granular Knudsen gas, we note that this gas does not depend much on the properties of its only boundary, which is the oscillatory region close to the plate.

The functional form of the horizontal velocity distribution in the steady-state region is nearly independent of height, when velocities are scaled by the local horizontal temperature (Fig. 6), even though the hydrodynamic fields continue to change. The distribution function is broader than the MB distribution, being underpopulated at small velocities and overpopulated in the high energy tails (Fig. 8). We do not observe a universal functional form for the distribution function (Fig. 9). The functional form of the high energy tail changes with the dissipation parameters (e and μ) and the oscillation parameter (V_{max}). The dependence on μ in the steady-state region is very weak (Fig. 10).

Our conclusions regarding the absence of a universal distribution function differ from that of Ref. [5], for the following reasons:

(1) We studied the local distribution function, while in Ref. [5] the authors studied the distribution function of grains in some range of height. Based on their observation of weak dependence of the *density* near the center of the oscillating box they assumed that a certain region near the center is homogeneous. Note that if a distribution is averaged over different *temperatures*, even the MB distribution function results in a different functional form.

(2) Our system is different from that in Ref. [5] as we do not have either air or sidewalls, and our container is much taller so that the bottom plate is the only energy source in our case. How air and sidewalls affect the dynamics of a granular gas is yet to be clarified.

We also studied the velocity distributions of frictionless inelastic hard spheres, and examined the possibility of including frictional effects using an effective normal coefficient of restitution. We found that no single effective restitution coefficient could describe the frictionless gas over a range of heights.

Velocities of a granular gas, even in the dilute limit, are strongly correlated, and the correlations depend on the density and the coefficient of restitution [24]. The dependence of

the distribution on the density implies that the single particle distribution of a dilute granular gas cannot play a role equivalent to that in a dilute ordinary gas; it is not sufficient to specify statistical properties of the gas. However, the knowledge of the single particle distribution of this complex nonequilibrium gas is still of great importance for the purpose of the first approximation.

ACKNOWLEDGMENTS

The authors thank J. Bougie, D. I. Goldman, E. Rericha, and J. van Zon for helpful discussions. This work was supported by U.S. Department of Energy Grant No. DE-FG-0393ER14312 and Texas Advanced Research Program Grant No. ARP-055-2001.

-
- [1] S. Warr, J.M. Huntley, and George T.H. Jacques, *Phys. Rev. E* **52**, 5583 (1995).
- [2] J.S. Olafsen and J.S. Urbach, *Phys. Rev. Lett.* **81**, 4369 (1998).
- [3] W. Losert, D.G.W. Cooper, J. Delour, A. Kudrolli, and J.P. Gollub, *Chaos* **9**, 682 (1999).
- [4] A Kudrolli and J. Henry, *Phys. Rev. E* **62**, R1489 (2000).
- [5] F. Rouyer and N. Menon, *Phys. Rev. Lett.* **85**, 3676 (2000).
- [6] J.J. Brey and M.J. Ruiz-Montero, *Phys. Rev. E* **67**, 021307 (2003).
- [7] A. Barrat and E. Trizac, *Phys. Rev. E* **66**, 051303 (2002).
- [8] C. Bizon, M.D. Shattuck, J.B. Swift, W.D. McCormick, and H.L. Swinney, *Phys. Rev. Lett.* **80**, 57 (1998).
- [9] S.J. Moon, M.D. Shattuck, C. Bizon, D.I. Goldman, J.B. Swift, and H.L. Swinney, *Phys. Rev. E* **65**, 011301 (2002).
- [10] S. J. Moon, J. Bougie, J. B. Swift, and H. L. Swinney (unpublished).
- [11] N. Maw, J.R. Barber, and J.N. Fawcett, *Wear* **38**, 101 (1976).
- [12] O.R. Walton, in *Particulate Two-Phase Flow*, edited by M.C. Roco (Butterworth-Heinemann, Boston, 1993), p. 884.
- [13] S.F. Foerster, M.Y. Louge, H. Chang, and K. Allia, *Phys. Fluids* **6**, 1108 (1994).
- [14] J. Bougie, S.J. Moon, J.B. Swift, and H.L. Swinney, *Phys. Rev. E* **66**, 051301 (2002).
- [15] M.Y. Louge and M.E. Adams, *Phys. Rev. E* **65**, 021303 (2002).
- [16] R. Soto, M. Mareschal, and D. Risso, *Phys. Rev. Lett.* **83**, 5003 (1999).
- [17] J.J. Brey, M.J. Ruiz-Montero, and F. Moreno, *Phys. Rev. E* **63**, 061305 (2001).
- [18] J. Lee, *Physica A* **219**, 305 (1995).
- [19] K. Huang, *Statistical Mechanics* (Wiley, New York, 1987).
- [20] M.N. Kogan, *Rarefied Gas Dynamics* (Plenum, New York, 1969).
- [21] T.P.C. van Noije and M.H. Ernst, *Granular Matter* **1**, 57 (1998).
- [22] N.V. Brilliantov and T. Pöschel, *Phys. Rev. E* **61**, 2809 (2000).
- [23] X. Nie, E. Ben-Naim, and S. Chen, *Phys. Rev. Lett.* **89**, 204301 (2002).
- [24] S.J. Moon, M.D. Shattuck, and J.B. Swift, *Phys. Rev. E* **64**, 031303 (2001).
- [25] D.L. Blair and A. Kudrolli, *Phys. Rev. E* **64**, 050301 (2001).
- [26] J.S. van Zon, D.I. Goldman, J. Kreft, J.B. Swift, and H.L. Swinney (unpublished).
- [27] S.J. Moon, J.B. Swift, and H.L. Swinney, *Phys. Rev. E* (to be published), e-print cond-mat/0308541.
- [28] S. Luding, *Phys. Rev. E* **52**, 4442 (1995).